Modeling Particle-Size Distribution Dynamics in a Flocculation System

Jian-jun Zhang and Xiao-yan Li
Environmental Engineering Research Center, Dept. of Civil Engineering, The University of Hong Kong, Hong Kong, China

Flocculation dynamics accounting for both particle coagulation and aggregate breakage was simulated mathematically by using modified sectional modeling techniques. The methodological improvement included the use of a continuous-size density function, instead of a characteristic size for each size section, the applications of a comprehensive curvilinear model for the coagulation kinetics, and the fractal scaling relationship for particle aggregates. Simulation results demonstrated that a flocculation system could arrive at a dynamic steady state after a period of flocculation when coagulation and breakage counterbalanced each other, resulting in a stationary size distribution with a unique peak mass concentration. Three distinct breakage distribution functions — binary, ternary, and normal distribution — did not differ considerably based on the simulation results of the steady-state size distributions. A lower shear rate, breakage rate constant, a higher collision efficiency, and initial particle concentration would result in larger aggregates in a flocculation system. The numerical simulations compared well with the results of the jar-test flocculation experiments using latex microspheres, suggesting the applicability of the curvilinear – fractal – breakage modeling system for the process simulation of the flocculation units used in water and wastewater treatment.

Introduction

Flocculation, which combines small particles into larger aggregates, is one of the most important unit operations in water and wastewater treatment. In water-treatment practice, flocculant sedimentation is commonly used for removing particulate impurities from water. In biological wastewater treatment, bio-flocs are formed in activated sludge aeration tanks and separated from effluent in secondary clarifiers. Despite the practical importance of flocculation in water and wastewater treatment, its mathematical modeling and simulation have not been well established. As there are numerous particles spun over a wide spectrum of sizes in a flocculation system, it is a difficult task to simulate the interactions between particles of various sizes and the transfer of particle matter among all sizes (Gardner et al., 1998). A number of issues also need to be addressed for a reliable mathematical simulation of particle flocculation. For example, in addition to coagulation that joins particles together into larger aggregates, breakage that breaks aggregates into smaller fragments plays an equally important role in regulating the size distribution of a particle population (Spicer and Pratsinis, 1996; Flesch et al., 1999). Both processes have to be included in the modeling of flocculation dynamics. For modeling the coagulation process, the curvilinear collision kernel, instead of the conventional but unrealistic rectilinear kernel, should be applied to describe the particle collision kinetics (Han and Lawler, 1992; O'Melia and Tiller, 1993; Thomas et al., 1999). As the aggregates formed by coagulation are fractal in structure, the fractal mass-size scaling relationship needs to be incorporated in the simulation of both the coagulation and breakage processes (Jiang and Logan, 1991; Jackson, 1998; Lee et al., 2000).

The mathematical modeling of flocculation usually makes use of the classic Smolchowski approach, in which the particle dynamics are simulated by the change in size distribution that is induced by simultaneous coagulation and breakage.

Correspondence concerning this article should be addressed to X.-y. Li.

Considerable progress has been made over the years in using numerical techniques to model the growth of particle sizes driven by coagulation (Thomas et al., 1999). A sectional method, which divides the whole particle-size range of concern into a manageable number of size sections, has been developed to solve the coagulation kinetic equations for the time evolution in size distribution (Gelbard et al., 1980; Hounslow et al., 1988; Jackson and Lochmann, 1993; Park and Lee, 2001). Attempts also have been made to incorporate the breakage process into flocculation models. In the early work of Fair and Gemmell (1964), aggregate breakage was included in a simple numerical study of flocculation, and the authors demonstrated the important role of breakage in a flocculation system. Through mathematical simulations, Boadway (1978) and Lu and Spielman (1985) found that shear-induced coagulation had to be combined with breakage to fit their experimental results. With detailed examination of the breakage phenomenon using the flow visualization technique, Pandya and Spielman (1982) further revealed the mechanisms of aggregate breakage in sheared fluid, and defined an elaborate model to describe the breakage kinetics. Using a numerical method for the breakage of large aggregates in a shear flow field, Higashitani et al. (2001) demonstrated that a power relationship holds between the average number of broken fragments and the intensity of fluid shear. In recent developments, the numerical approach has been further improved, which uses the sectional approximation in combination with simplified breakage functions to simulate particle flocculation, accounting for both coagulation and breakage (Vigil and Ziff, 1989; Cohen, 1992; Spicer and Pratsinis, 1996; Kostoglou et al., 1997; Dasgupta, 2000). It has been demonstrated that there is a steady-state particle-size distribution in a batch flocculation system. The characteristic time for the system to arrive at its steady state and the corresponding steady-state size distribution are unique for a given flocculation system (Spicer and Pratsinis, 1996; Chung et al., 1998; Flesch et al., 1999).

Although simulation studies have provided valuable findings for better understanding of flocculation dynamics, the exact results of most numerical simulations are apparently rather questionable. Deficiencies can still be identified in the method of flocculation modeling. For example, a characteristic size, such as the arithmetic average of the lower and upper boundary sizes of a section (Spicer and Pratsinis, 1996), has been used to represent all particles in the size section. In this simplification, particles lose their continuous-size spectrum and are grouped into a number of discrete characteristic sizes. This treatment is applicable only when narrow sections are used, and it becomes inaccurate as the width of sections increases (Patil et al., 1997). The rectilinear collision model, which has been known to overpredict collision frequencies between particles (Han and Lawler, 1992; Veerapaneni and Wiesner, 1996; Li and Logan, 1997), is still used to model the coagulation process. For the description of aggregate breakage, a number of formulations of fragment distribution functions are currently available, such as binary, ternary, and normal distribution functions. The differences between these functions have not been fully examined. In addition, the influences of various important process parameters, such as the shear rate, collision efficiency between particles, the initial concentration, and the breakage-rate coefficient, on the steady-state size distribution of a flocculation system have not been well determined through numerical simulations. More experimental studies also are needed to evaluate the results of modeling simulations.

With the introduction of fractal geometry for the particle aggregates formed by coagulation, the mathematical description of the flocculation process has been largely revised (Li and Ganczarczyk, 1989; Jiang and Logan, 1991; Jackson, 1998; Lee et al., 2000). Fractal aggregates have much larger sizes than the otherwise coalesced spherical particles, which enhances both coagulation between particles and the breakage of aggregates. In our present study, we established a modeling system to simulate particle flocculation dynamics. The fractal scaling characteristics of particle aggregates were incorporated in modeling the breakage behavior of particles and the interactions between particles. An improved sectional approach developed by Jackson and coworkers (Jackson and Lochmann, 1993; Jackson, 1998) was adopted to more properly integrate the Smoluchowski equation. This sectional method is based on the realistic assumption that particles within a section have a continuous-size distribution that satisfies a size density function. A curvilinear collision model developed by Han and Lawler (1992), which is by far the most complete and comprehensive curvilinear function, was used for the coagulation kinetics. With the advanced curvilinear–fractal–breakage model, numerical simulations were carried out for the particle flocculation dynamics. In addition, laboratory experiments of batch flocculation were conducted to verify the results of numerical simulations in terms of the particle-size distribution after flocculation.

Methodology

Coagulation and breakage kinetics

The flocculation dynamics in a system of heterodisperse particles can be modeled by the change in particle-size distribution. When both particle coagulation and aggregate breakage are considered, the kinetics for the change in the size distribution can be described (Spicer and Pratsinis, 1996; Chung et al., 1998; Flesch et al., 1999) below in the form of the Smoluchowski equation

$$\frac{dn(m)}{dt} = \frac{1}{2}\int_0^m \alpha\beta(m-m',m')n(m-m')n(m')\,dm' - n(m)\int_0^\infty \alpha\beta(m,m')n(m')\,dm' - s(m)n(m) + \int_m^\infty \gamma(m,m'')s(m'')n(m'')\,dm'' \quad (1)$$

where t is time; $n(m)$ is the particle-size density function with respect to the particle size measured by mass, m; β is the collision frequency function describing the rate of particle contacts; α is the collision efficiency; m' is the mass of a particle smaller than m that upon collision with a particle of size $m-m'$ forms a particle of mass m; $s(m)$ is the breakup rate function of the aggregates of size m; and $\gamma(m,m'')$ is the breakage distribution function defining the mass fraction of the fragments of size m breaking from the larger aggregates of size m''. The first term on the righthand side of Eq. 1

represents the gain term for the particles of size m by coagulation between smaller particles. The second term is for the loss of particles of size m due to their growth in size by attachment with other particles. The third term is for the loss of the aggregates of size m as the results of breakage, and the fourth term is for the gain of particles of size m from the fragments of broken aggregates.

To solve Eq. 1, which represents a family of complex integrodifferential equations, the numerical technique with sectional approximation needs to be applied (Gelbard et al., 1980; Hounslow et al., 1988). Following the common practice of the sectional method (Gelbard et al., 1980; Jackson and Lochmann, 1993; Jackson, 1998; Li and Zhang, 2003), the size sections are so generated that the upper bound of a section is twice its lower bound in terms of particle mass, that is, $m_k = 2m_{k-1}$. Within each size section, it is assumed here that the particle mass distributes uniformly along the log-scale, that is, $\Delta M/\Delta(\log\ m) = \text{constant}$, or $dM/d(\log\ m) = (\ln 10)m^2 n(m) = \text{constant}$ (Seinfeld, 1986), where M is the cumulative mass distribution. Since the total mass concentration in the kth section is $Q_k = \int_{m_{k-1}}^{m_k} mn(m)\ dm$, the particle-size density function, $n(m)$, can be derived as

$$n(m) = \frac{Q_k}{(\ln 2)m^2} \tag{2}$$

Sectional governing equations

Attachment between two particles of masses m_x and m_y from sections i and j, respectively, where $m_x \le m_y$, can move the mass into or out of the kth section. Breakage of the particle aggregates of mass m in the kth section and those of the mass m_z that is larger than m can also move the mass into or out of the kth section, respectively. These simultaneous coagulation and breakage actions regulate the change of the particle mass concentration in a section. With the treatment of the sectional method, Eq. 1 can be converted into a kinetic expression of Eq. 3, for the particle mass in section k. Transformation from Eq. 1 to the new governing equation can be found in detail elsewhere (Gelbard et al., 1980; Jackson, 1998; Li and Zhang, 2003). For any given section, for example, the kth section, there are a total of seven cases of coagulation and breakage involved in the mass movement. Table 1 illustrates these seven particle interactions resulting in the gain and loss of particle mass in the kth section, where s signifies the last size section. ${}^1B_{i,k-1,k}$, ${}^2B_{i,k,k}$, ${}^3B_{i,k,k}$, ${}^4B_{k,k,k}$, and ${}^5B_{k,i,k}$ are the sectional coagulation coefficients, and ${}^1S_k$ and ${}^2S_{k,i}$ are the sectional breakage coefficients. The computation of these coefficients is also summarized in Table 1.

$$\begin{aligned}\frac{dM_k}{dt} = {} & M_{k-1}\sum_{i=1}^{k-1} {}^1B_{i,k-1,k}M_i + M_k\sum_{i=1}^{k} {}^2B_{i,k,k}M_i \\ & - M_k\sum_{i=1}^{k} {}^3B_{i,k,k}M_i - {}^4B_{k,k,k}M_k^2 \\ & - M_k\sum_{i=k+1}^{s} {}^5B_{k,i,k}M_i - {}^1S_kM_k + \sum_{i=k+1}^{s} {}^2S_{k,i}M_i\end{aligned} \tag{3}$$

As k varies from 1 to s, Eq. 3 represents a finite number of coupled ordinary differential equations for the rates of mass transfer between all of the size sections. Thus, the simultaneous coagulation and breakage dynamics can be simulated by solving these equations for the time evolution of particle-size distributions. In the present study, the fourth-order Runge–Kutta method has been employed for the numerical integration of Eq. 3. As shown in Table 1, the sectional coagulation and breakage coefficients are independent of time and mass concentration; thus, their calculations need to be conducted only once before the computation of mass exchange between sections.

Fractal and fractal aggregates

Although mass is the property conserved in particle attachment and aggregate breakage, the actual length determines more directly the particle behaviors and the interactions between particles. Particle aggregates, which have been characterized as fractals (Meakin, 1988; Li and Ganzarczyk, 1989; Jiang and Logan, 1991; Li and Logan, 1995), are highly porous and irregular in shape. For fractal aggregates, their masses and lengths l can be related according to $m \sim l^D$, where D is the fractal dimension. The actual length of an aggregate may be obtained from the mass (Jiang and Logan, 1991; Li and Logan, 1995) using

$$l = c\left(\frac{m}{\rho_p}\right)^{1/D} \tag{4}$$

where ρ_p is the density of primary particles, and c is an empirical constant. The settling velocity of a fractal aggregate with a density of ρ_a can be calculated using Stokes' law $U = (g(\rho_a - \rho_l)l^2)/18\mu$, or

$$U = \frac{g(\rho_p - \rho_l)m}{3\pi\mu\rho_p l} \tag{5}$$

where g is the gravitational constant, ρ_l is the density of the liquid, and μ is the fluid viscosity (Johnson et al., 1996; Li and Yuan, 2002).

Breakage rate and breakage distribution functions

The breakup of aggregates in water is brought about mainly by hydrodynamic stresses, such as fluid shear (Tambo and Hozumi, 1979; Peng and Williams, 1994; Serra and Casmitjana, 1998a,b; Kramer and Clark, 1999; Higashitani et al., 2001). The fragility of an aggregate is generally proportional to its size—as the aggregate increases in size, it becomes more vulnerable to breakage (Pandya and Spielman, 1982; Potanin, 1991; Yeung and Pelton, 1996; Spicer et al., 1998). Based on the understanding of the breakage mechanisms, the breakage rate coefficient can be written as a function of the shear rate, G, and the aggregate size in volume, V (Chen et al., 1990; Peng and Williams, 1994; Flesch et al., 1999), or

$$s(V) = EG^bV^{1/3} \tag{6}$$

where E and b are the breakage rate constants. A pair of $E = 7.0\times10^{-4}$ and $b = 1.6$ have been successfully used by

Table 1. Different Coagulation and Breakage Cases and Related Sectional Coefficients

Case	Symbol	Description	Illustration	Calculation $f(m_x,m_y) = \frac{\alpha\beta(m_x,m_y)}{(\ln 2)^2 m_x^2 m_y^2}$
1 Gain	${}^{1}B_{i,j,k}$	Newly formed doublets moving into the kth section, $m_{k-1} < (m_x + m_y) < m_k$; $m_0 \le m_x \le m_{k-1}$ and $m_{k-2} \le m_y < m_{k-1}$; $i \le k-1$, $j = k-1$.	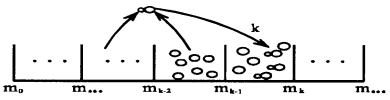	$\int_{m_{i-1}}^{m_i}\int_{m_{k-1}-m_x}^{m_{k-1}} (m_x + m_y) \times f(m_x,m_y)\, dm_x\, dm_y$ $\frac{1}{2}\int_{m_{k-2}}^{m_{k-1}}\int_{m_{k-2}}^{m_{k-1}} (m_x + m_y) \times f(m_x,m_y)\, dm_x\, dm_y$
2 Gain	${}^{2}B_{i,j,k}$	Newly formed doublets remaining in the kth section, $m_{k-1} < (m_x + m_y) < m_k$; $m_0 \le m_x < m_{k-1}$ and $m_{k-1} \le m_y < m_k$; $i < k$, $j = k$.	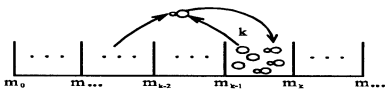	$\int_{m_{i-1}}^{m_i}\int_{m_{k-1}}^{m_k - m_x} m_x f(m_x,m_y) \times dm_x\, dm_y$
3 Loss	${}^{3}B_{i,j,k}$	Particles being moved out of the kth section by attachment to smaller particles, $m_k < (m_x + m_y)$; $m_0 \le m_x < m_{k-1}$ and $m_{k-1} \le m_y < m_k$; $i < k$, $j = k$.	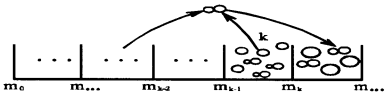	$\int_{m_{i-1}}^{m_i}\int_{m_{k-1}}^{m_k - m_x} m_y f(m_x,m_y) \times dm_x\, dm_y$
4 Loss	${}^{4}B_{i,j,k}$	Particles being moved out of the kth section by attachment to similarly sized particles, $m_k < (m_x + m_y)$; $m_{k-1} \le m_x < m_k$ and $m_{k-1} \le m_y < m_k$; $i = k$, $j = k$.	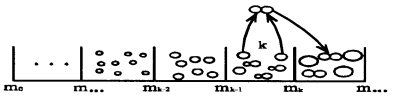	$\frac{1}{2}\int_{m_{k-1}}^{m_k}\int_{m_{k-1}}^{m_k} (m_x + m_y) \times f(m_x,m_y)\, dm_x\, dm_y$
5 Loss	${}^{5}B_{i,j,k}$	Particles being moved out of the kth section by attachment to larger particles, $m_k < (m_x + m_y)$; $m_{k-1} \le m_x < m_k$ and $m_k \le m_y$; $i = k$, $k < j$.	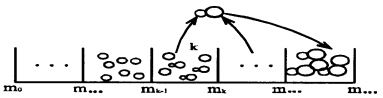	$\int_{m_{k-1}}^{m_k}\int_{m_{j-1}}^{m_j} m_y f(m_x,m_y) \times dm_x\, dm_y$
6 Loss	${}^{1}S_k$	Particles being moved out of the kth section by breakage, $m_{k-1} < m < m_k$.	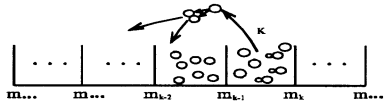	$\int_{m_{k-1}}^{m_k} \frac{s(m)}{m \ln 2}\, dm$
7 Gain	${}^{2}S_{k,i}$	Particle fragments moving into the kth section by breakage of larger particles, $m_{k-1} < m < m_k$ and $m_{i-1} < m_z < m_i$; $k < i$.	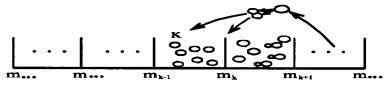	$\int_{m_{k-1}}^{m_k}\int_{m_{i-1}}^{m_i} \frac{\gamma(m,m_z)s(m_z)}{m_z \ln 2} \times dm_z\, dm$

Flesch et al. (1999) to fit the data of Oles (1992) and their own experimental studies. These values therefore are adopted in the present numerical simulation. Using the fractal scaling correlation of Eq. 4 and $V = (\pi/6)l^3$, Eq. 6 can be converted below as a function of the shear rate and particle mass

$$s(m) = E'G^{1.6}m^{1/D} \tag{7}$$

where

$$E' = \left(\frac{\pi}{6}\right)^{1/3}\left(\frac{1}{\rho_p}\right)^{1/D} cE$$

There are generally three distinct breakage distribution functions, binary, ternary, and normal distribution, that have been used to describe the fractions of the fragments of size m breaking from the larger aggregates of size m'' (Coulaloglou and Tavlarides, 1977; Chen et al., 1990; Spicer and Pratsinis, 1996; Flesch et al., 1999). Binary breakage means the breakup of an aggregate into two equal fragments, which has a distribution form of

$$\gamma(m,m'') = \begin{cases} 2 & (m = m''/2) \\ 0 & (m \ne m''/2) \end{cases} \tag{8}$$

Ternary breakage describes the breakup of an aggregate into two equal fragments, and one of the fragments breaking further into two equal and smaller pieces. This distribution function can be written as

$$\gamma(m,m'') = \begin{cases} 2 & (m = m''/4) \\ 1 & (m = m''/2) \\ 0 & (m \ne m''/4, m''/4) \end{cases} \tag{9}$$

Normal breakage produces a normal-size distribution of the fragments, which can be described as

$$\gamma(m,m'') = \frac{m''}{m}\int_{m_{k-1}}^{m_k} \frac{1}{\sigma_f\sqrt{2\pi}}\exp\left[-\frac{(m-m_f)^2}{2\sigma_f^2}\right]dm \quad (10)$$

where m_f is the mean mass and σ_f is the standard deviation of the fragment-size distribution. Following previous studies (Coulaloglou and Tavlarides, 1977; Spicer and Pratsinis, 1996), $m_f = m''/2$ and $\sigma_f = m''/10$ are assumed in the present simulation, which give a relatively narrow fragment distribution around the half-size of the broken aggregates.

Coagulation kernels

Particles in water are brought into contact by three different collision mechanisms: Brownian motion, fluid shear, and differential sedimentation. Several models with different levels of accuracy have been developed to describe the collision frequency functions. The rectilinear model, which assumes that particles move in straight lines until collisions occur, has the following formulations:

For Brownian motion

$$\beta_{Br}(i,j) = \frac{2kT}{3\mu}\left(\frac{1}{l_i}+\frac{1}{l_j}\right)(l_i+l_j) \quad (11)$$

where k is Boltzmann's constant and T is the absolute temperature.

For fluid shear

$$\beta_{Sh}(i,j) = \frac{G}{6}(l_i+l_j)^3 \quad (12)$$

For differential sedimentation

$$\beta_{DS}(i,j) = \frac{\pi}{4}(l_i+l_j)^2|U_i-U_j| \quad (13)$$

The three interparticle collision frequency functions are independent and additive, that is

$$\beta(i,j) = \beta_{Br}(i,j)+\beta_{Sh}(i,j)+\beta_{DS}(i,j) \quad (14)$$

The curvilinear collision model takes into account hydrodynamic interactions and short-range forces between approaching particles, which results in reduced, but likely more realistic, collision frequencies. Accurate analytical expression of the curvilinear model, however, is not readily available. Han and Lawler (1992) made a considerable effort to solve the curvilinear interactions between approaching particles and provided by far the most comprehensive set of numerical solutions for the three collision mechanisms. They related the curvilinear β_{cur} to the well-defined rectilinear β by the reduction factors, that is

$$\beta_{cur}(i,j) = e_{Br}\beta_{Br}(i,j)+e_{Sh}\beta_{Sh}(i,j)+e_{DS}\beta_{DS}(i,j) \quad (15)$$

where e_{Br}, e_{Sh}, and e_{DS} are the curvilinear reduction factors for the collision mechanisms indicated. According to Han and Lawler (1992), these factors can be estimated by

$$e_{Br} = a+b\lambda+c\lambda^2+d^3 \quad (16)$$

$$e_{Sh} = \frac{8}{(1+\lambda)^3}10^{(a+b\lambda+c\lambda^2+d\lambda^3)} \quad (17)$$

$$e_{DS} = 10^{(a+b\lambda+c\lambda^2+d\lambda^3)} \quad (18)$$

where λ is the size ratio ($0<\lambda\le 1$) between the two approaching particles, and a, b, c, and d are the intermediate coefficients. Although the same letters are used here, the coefficients of a, b, c, and d differ completely in the three equations. In Han and Lawler's results, these intermediate coefficients are written as the functions of l_l, H_A, and N_g for e_{Br}, e_{Sh}, and e_{DS}, respectively, where l_l is the length of the larger one of the two particles, $H_A = A/(18\pi\mu l_l^3 G)$ and $N_g = 48A/(\pi g(\rho_a-\rho_l)l_l^4)$, and A is the Hamaker constant. The values of a, b, c, and d were given by Han and Lawler (1992) in three tables for the three collision mechanisms. To make their results more available for use in mathematical simulation, nonlinear regression was performed to transform the discrete data into analytical formulations. The derivation and results of the fitting equations for the coefficients of a, b, c, and d used in computation of the curvilinear reduction factors in Eqs. 16–18 can be found in Li and Zhang (2003).

Modeling and simulation conditions

Mathematical simulations of the particle coagulation–breakage process were performed for a batch flocculation system with a pulse input of monomers into water. The primary particles were 1 μm in diameter with a density of 1.2 $g\cdot cm^{-3}$. The initial particle concentrations of $Q_0 = 5.0\times 10^{-5}$, 1.0×10^{-4}, 2.5×10^{-4}, and 5.0×10^{-4} $g\cdot cm^{-3}$ were examined. The whole size range was from 1 μm to approximately 1 cm for nonfractal particles, which extended further for fractal particle aggregates. There were 42 contiguous-size sections with the setting of $m_k = 2m_{k-1}$ for the lower and upper bounds of a section as defined earlier. The initial condition of the simulation can be written as

$$\begin{cases} Q_1(t=0) = Q_0 \\ Q_k(t=0) = 0 \quad (k=2,3,\ldots,42) \end{cases} \quad (19)$$

Continuous stirring was applied to the system to promote both particle collisions and aggregate breakage. It was assumed that no particle mass was lost from the solution to sedimentation. Three degrees of fluid shear, $G = 15$, 50, and 150 s^{-1}, were tested in the simulations.

In addition, the following assumptions were made for the flocculation system: the particles and aggregates had a uniform collision efficiency, and all particle aggregates formed by coagulation had the same fractal dimension throughout the size distribution. Other coefficients and constants included: the temperature $T = 25°C = 298$ K; liquid density $\rho_l = 1.0$ $g\cdot cm^{-3}$; viscosity $\mu = 8.9\times10^{-3}$ $g\cdot cm^{-1}\cdot s^{-1}$, Boltzmann's constant $k = 1.38\times10^{-16}$ $g\cdot cm^2\cdot s^{-2}\cdot K^{-1}$; the Hamaker constant $A = 4.0\times10^{-13}$ $g\cdot cm^2\cdot s^{-2}$; and the gravitational constant $g = 981$ $cm\cdot s^{-2}$.

Experimental study

Batch flocculation experiments using a jar-test device (PB-700, Phipps & Bird) were conducted with standard red-dyed latex microspheres of 3.0 μm in diameter with a density of 1.05 $g \cdot cm^{-3}$ (Polysciences). The standard particles were placed in a 600-mL beaker filled with 500 mL 3.5% NaCl solution. Two different initial concentrations of the primary particles, $Q_0 = 5.0 \times 10^{-5}$ and 1.0×10^{-4} $g \cdot cm^{-3}$, were used. A flat mixing paddle (7.6×2.5 cm^2) was rotated at either 25 or 60 rpm, which resulted in two different shear rates of $G =$ 15 and 50 s^{-1} according to the calibration of Li and Logan (1997). Alum ($Al_2(SO_4)_3 \cdot 18H_2O$) was added as the flocculent at a concentration of either 10 or 30 mg/L, while 0.1 M $NaHCO_3$ was used to adjust the solution pH.

Following the techniques used by Li and Logan (1997) and Li and Zhang (2003), three different cases of flocculation —slow, normal, and fast— were obtained by adjusting the operation and water chemistry conditions. For the normal flocculation case, alum was dosed at 10 mg/L, and the solution pH was maintained at around 7.5. For the relatively slow flocculation, the same amount of alum was dosed, and the solution pH was around 6.0 without any adjustment. For the fast flocculation case, a higher alum dosage of 30 mg/L was applied, and the pH was adjusted to around 7.5. During the fast flocculation, rapid aggregate formation was observed and the system reached the stationary stage in terms of aggregate formulation within 1 h at a shear rate of 50 s^{-1}. For the normal flocculation, the system became stationary within 2 h or so. For the slow flocculation, aggregates formed at a much slower rate and the system approached a stationary state after 8 h. According to previous studies under similar conditions (Jiang and Logan, 1996; Li and Logan, 1997; Li and Zhang, 2003), the particles that underwent the fast flocculation were likely to be fully destabilized, and the aggregates formed were expected to be more fractal. Thus, $\alpha = 1.0$ and $D = 2.0$ were assumed for this flocculation case. For the normal flocculation case, particles were partially destabilized and the aggregates were less fractal. Thus, $\alpha = 0.8$ and $D = 2.2$ were assumed. Accordingly, $\alpha = 0.4$ and $D = 2.5$ were assumed for the slow flocculation case. These values were used in the mathematical simulation of the batch flocculation systems, and the simulation results were compared to the experimental observations.

For each run of the coagulation–breakage experiments, samples were gently withdrawn from the particle suspension using microbiological counting cells (Graticules, London) at various time intervals. Each counting cell has an effective volume of 1 mL with a dimension of $5 \times 2 \times 0.1$ cm^3. The sample in a cell was placed under a microscope (BX60, Olympus) that was equipped with a digital camera (DP10, Olympus) and a computer-based image-analysis system (Scion Image). Projected images of the particles in the sample under a bright light were analyzed by the image software for particle sizing and counting following the procedures that have been detailed elsewhere (Li and Logan, 1995). Forty fields were scanned at 200× for each sample to obtain its particle-size distribution.

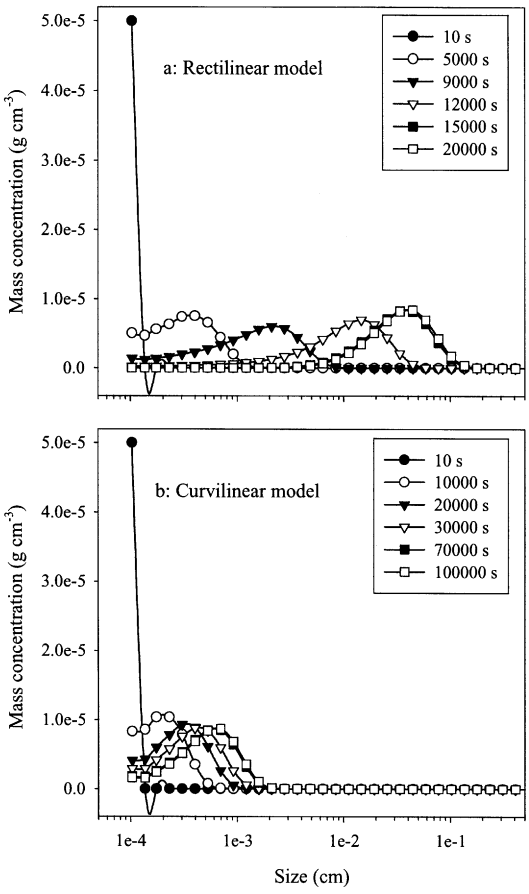

Figure 1. Evolution of particle-size distributions in a coagulation breakage system as simulated by (a) rectilinear model and (b) Han and Lawler's curvilinear model.

$D = 2.5$, $\alpha = 0.1$, $G = 50$ s^{-1}, and $Q_0 = 5 \times 10^{-5}$ $g \cdot cm^{-3}$.

Results and Discussion

Particle-size distribution at the dynamic steady state

The dynamics of simultaneous particle coagulation and aggregate breakage were well simulated, as demonstrated by the time evolution in particle-size distribution (Figure 1). For a pulse input of particles in a solution, the batch flocculation system could reach its dynamic steady state in terms of the size distribution after a period of simulation. In the early phase of the process, coagulation was predominant in relation to breakage, which moved the distribution toward larger sizes. As coagulation proceeded, aggregates become larger and more fragile, and breakage that decelerated the continuous growth of particle sizes became increasingly important. After a period of simulation—about 20,000 s for the rectilinear model and 100,000 s for the curvilinear model—the particle-size distributions did not show any significant change. Equilibrium between coagulation and breakage was eventually achieved in the flocculation system. Further examination of the differences between the rectilinear and curvilinear collision models is given in the section below. In the dynamic steady state, the particle-mass-size distribution was unimodal in shape with a peak concentration. This result is typical of the simultaneous coagulation and breakage processes and has been demonstrated by previous laboratory studies (Oles, 1992;

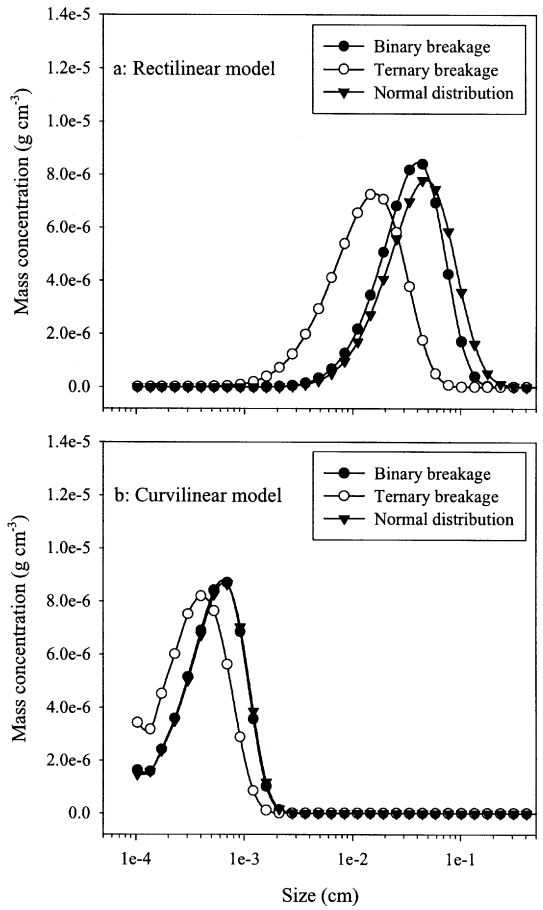

Figure 2. Comparisons of three fragment-distribution functions, binary, ternary, and normal distribution for the breakage process in terms of the simulation result of the dynamic steady-state size distributions in a flocculation system using (a) rectilinear model and (b) Han and Lawler's curvilinear model.

$D = 2.5$, $\alpha = 0.1$, $G = 50\ s^{-1}$, and $Q_0 = 5 \times 10^{-5}\ g \cdot cm^{-3}$.

Kusters et al., 1993; Chaignon et al., 2002) and the experimental results below.

The steady-state particle-size distributions that were simulated from the three distinct breakage distribution functions —binary, ternary, and normal distribution—compared fairly well with one another. For both the rectilinear (Figure 2a) and curvilinear (Figure 2b) collision models, the size distributions predicted from the binary and normal breakage functions nearly overlaid each other. The ternary breakage produced a distribution in smaller sizes within a slightly wider size range when compared to the cases of the binary and normal breakages. Considering the physical process of the breakage of an aggregate in section k, all of the fragments fell into section k-1 based on the binary breakage function. For the ternary breakage, however, only half of the fragment mass moved into section k-1, and the other half moved further down to section k-2. For the normal breakage function, half of the section k aggregate, which was actually within section k-1, was used as the mean size of the fragments. With the narrow standard deviation used in the study, most of the fragments would concentrate in section k-1, which is similar to the situation of binary breakage. Therefore, the simulation's use of the binary and normal breakage functions produced rather similar steady-state size distributions (Figure 2). Although the normal breakage function is considered to be a more realistic description of the fragment size distribution (Coulaloglou and Tavlarides, 1977; Spicer and Pratsinis, 1996; Flesch et al., 1999), the binary breakage was used in the following simulation studies because of its simplicity.

Coagulation kernels and fractal dimension

The rectilinear and curvilinear models showed patterns that were comparable with each other in the evolution of particle-size distributions from the same initial condition. However, the flocculation system arrived at the dynamic steady state at a much faster rate when based on the rectilinear model than when based on the curvilinear model (Figure 1). In addition, there were many more large particles in the rectilinear model-based system than in the curvilinear model-based system (Figure 2). While the curvilinear model is more accurate for the collision kinetics, the rectilinear model overpredicts the rate of particle coagulation (Han and Lawler, 1992; Veerapaneni and Wiesner, 1996; Li and Logan, 1997; Thomas et al., 1999). When the rectilinear model was used, coagulation could be greatly accelerated, which led to a shorter time before arrival at the steady state in comparison to the simulation with the more realistic curvilinear model. The collision models, on the other hand, did not affect the description of the breakage kinetics. Thus, as coagulation proceeded at an unrealistically faster rate with the rectilinear model, the balance between coagulation and breakage shifted the steady-state size distribution toward larger sizes. Considering the remarkable difference between the two collision models in the simulation results, the curvilinear model, instead of the conventional rectilinear model, should be used to model the coagulation process in particle flocculation.

Fractal scaling also needs to be incorporated into the modeling procedure for the flocculation simulation. As the fractal dimension decreased from 3 to 2.2 for the curvilinear model, the size of peak concentration increased from 3 μm to 10 μm, and the peak concentration decreased from 1.0×10^{-5} $g \cdot cm^{-3}$ to 7.5×10^{-6} $g \cdot cm^{-3}$ (Figure 3a). The same tendency occurred in the simulation that used the rectilinear model. The size of the peak concentration increased from 20 μm to nearly 20 cm as the fractal dimension decreased from 3 to 2.2. The rectilinear model is certainly more sensitive than the curvilinear model to the magnitude of fractal dimension. For the same change in the fractal dimension, the peak size increased four orders of magnitude according to the rectilinear model, in comparison to an increase of about three times based on the curvilinear model.

The fractal dimension is an essential parameter in the characterization of the scaling relationship of particle aggregates (O'Melia and Tiller, 1993; Li and Logan, 1995; Jiang and Logan, 1996; Jackson, 1998). When the fractal nature of particles is considered, aggregates become more porous and much larger than the otherwise coalesced particles of the same mass. Both the coagulation and breakage rates increase with the size of the particles. However, the coagulation rate increased exponentially with the particle size, for example, to

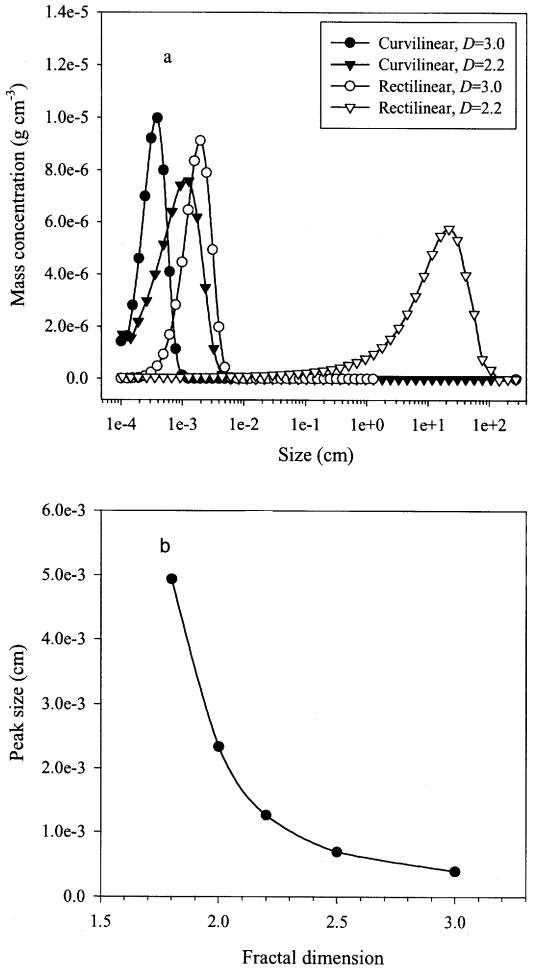

Figure 3. (a) Steady-state size distributions of particles in a flocculation system simulated by rectilinear and curvilinear models with different fractal dimensions; (b) change of the size of the peak mass concentration as a function of the fractal dimension simulated using Han and Lawler's curvilinear model.

$\alpha = 0.1$, $G = 50\ s^{-1}$, and $Q_0 = 5 \times 10^{-5}\ g \cdot cm^{-3}$.

a power of 3 for shear coagulation, while the breakup rate increases only linearly with the particle size. Thus, as the fractal dimension decreases, with the ever-increasing particle size, the coagulation rate increases more rapidly than does the breakage rate. This forced the particle population toward larger sizes in the size distribution. As the fractal dimension decreased from 3.0 to 2.5, 2.0, and 1.8, according to the simulation with the curvilinear model, the peak size increased from 4 to 7, 23, and 50 μm (Figure 3b). Therefore, consistent with many previous studies (Kuster et al., 1993; Jackson, 1998; Adachi et al., 1998), the present simulations further exhibited the important role of the fractal dimension in regulating the flocculation dynamics and steady-state particle-size distribution. A recent laboratory study by Flesch et al. (1999) found that a fractal dimension of $D = 2.05$ must be incorporated into the coagulation and breakage model to reconcile the experimental results of batch flocculation using polystyrene particles.

Effects of the shear rate, collision efficiency, and initial concentration

A lower shear rate, higher collision efficiency, and higher initial particle concentration resulted in a steady-state size distribution with more large-particle aggregates (Figure 4). An increase in the shear rate will increase the rate of particle coagulation, but it will also increase the rate of aggregate breakage. When the shear rate increased from 15 to 50 and 150 s^{-1}, the peak size decreased from 200 to 70 and 30 μm (Figure 4a). Within the range of shear rate examined here, the fluid shear appeared to play a negative role in the formation of large aggregates. As anticipated, a higher collision efficiency between particles increased the coagulation rate, resulting in a distribution with more aggregates of larger sizes. As the α increased from 0.1 to 0.3 and 1.0, the size of the peak concentration increased from 60 to 200 and 600 μm (Figure 4b). An increase in the initial particle input also made the condition more favorable to aggregate formation. When

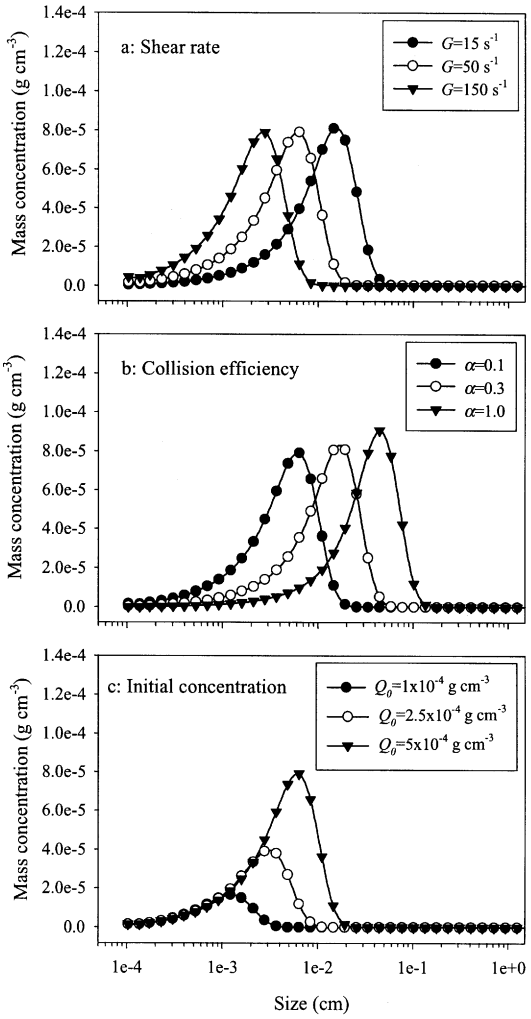

Figure 4. Effects of the process variables on the population dynamics in a flocculation system.

(a) The shear rate: $\alpha = 0.1$, $Q_0 = 5 \times 10^{-4}\ g \cdot cm^{-3}$; (b) the collision efficiency between particles: $G = 50\ s^{-1}$, $Q_0 = 5 \times 10^{-4}\ g \cdot cm^{-3}$, and (c) the initial particle concentration: $\alpha = 0.1$, $G = 50\ s^{-1}$. The curvilinear model was used in the simulation and $D = 2.5$.

the particle concentration increased from 1.0×10^{-4} to 2.5×10^{-4} and 5.0×10^{-4} g cm^{-3}, the peak size increased almost linearly from 15 to 32 and 60 μm (Figure 4c). A higher initial concentration produced more large aggregates with a higher peak concentration when the dynamic steady state was achieved.

For a particle population with a predominant size in a flocculation system, the particle mass is driven in opposite directions by the two processes. Coagulation grows particles into larger sizes, and breakage divides the particles into small fragments. Chung et al. (1998) introduced two dimensionless groups in shear flocculation to characterize the two tendencies of the mass transfer along the size distribution: $\eta_c = \alpha\phi G t_0$ for the size growth by coagulation and $\eta_b = EG^{1.6}V^{1/3}t_0$ for the size decrease by breakage, where ϕ is the particle concentration in volume fraction and t_0 is the characteristic time for the flocculation system to reach its steady state. It can be further predicted that coagulation and breakage will counterbalance each other when $\eta_c = \eta_b$, which will result in a steady-state system with a predominant size class that no longer changes with time. If the fractal structure of particle aggregates is not considered, then it can be written that $\phi = p_1 Q_0$ and $V^{1/3} = p_2 d_s$, where Q_0 is the particle mass concentration, d_s is the solid equivalent diameter of the particle aggregates, and p_1 and p_2 are constants. For a flocculation system that is arriving at its steady state, it can be derived from $p_1\alpha Q_0 G t_0 = p_2 EG^{1.6} d_s t_0$ that $d_s = p_1\alpha Q_0/p_2 EG^{0.6}$. When the fractal property of the particle aggregates is incorporated, the fractal scaling relationship of Eq. 4 gives $l \sim d_s^{3/D}$. Thus, we have

$$l = p\left(\frac{\alpha Q_0}{EG^{0.6}}\right)^{3/D} \tag{20}$$

where p is an overall constant.

Equation 20 suggests that the operational variables, including the collision efficiency, initial concentration, shear rate, and breakage constant, can be grouped into a single universal parameter, $\alpha Q_0/EG^{0.6}$, which eventually regulates the predominant size of the particles in a flocculation system. The effect of the fractal dimension on the peak size of a distribution is also included in Eq. 20. By varying the variables of α, G, Q_0, and E, additional numerical simulations were carried out and various peak sizes in the particle systems resulted. Plotting the peak size as a function of $\alpha Q_0/EG^{0.6}$ after log-log transformation, it can be seen that the peak size increases linearly with the group parameter to a power of approximately $3/D$ (Figure 5). This correlation obtained from the simulations is in excellent agreement with the theoretical prediction of Eq. 20. Therefore, this group parameter provides a general guideline for the operation and improvement of particle flocculation systems. When the value of $\alpha Q_0/EG^{0.6}$ increases, which means that the collision efficiency and initial concentration increase and the shear rate decreases, the steady-state size distribution will move toward larger sizes with more large aggregates.

Chaignon et al. (2002) recently examined the coagulation and breakage behavior of activated sludge flocs by monitoring the changes of the floc size distribution under various conditions of fluid agitation and sludge concentration. They observed that the mean floc size changed from 125 to 75 and back to 125 μm as the stirring rate changed from 100 to 200 and then to 100 rpm at a sludge concentration of 3.5×10^{-5} g cm^{-3}. At a constant shear rate of $G = 135$ s^{-1}, the mean floc size increased almost linearly with the activated sludge concentration. As the sludge concentration increased from 3.5×10^{-5} to 7.0×10^{-5} and 1.4×10^{-4} g·cm^{-3}, the mean floc size grew from 95 to 115 and 135 μm. These experimental observations are consistent with the theoretical relationship suggested by Eq. 20 and Figure 5. In more general terms, the simulation results for the effect of operational conditions on particle flocculation are well in line with common experiences in water supply and treatment processes. For example, in drinking water treatment, the flocculation of a turbid raw water influent is usually less difficult than that of a clean rate water influent with a low turbidity (Packham, 1965; Amirtharajah and O'Melia, 1990). For the water of a low turbidity, flocculants often have to be overdosed to form chemical precipitates that remove particulate impurities from water by enmeshment. In this practice, flocculants increase the collision efficiency between particles, and the precipitates of flocculants increase the solid content in water. Both are favorable factors for particle flocculation according to the preceding simulation. As another major control variable in water treatment, the shear rate is usually so designed that it gradually decreases throughout the flocculation process (Amirtharajah and O'Melia, 1990; American Water Works Association, 1998), for example, from $G = 1{,}000$ to 100 and 20 s^{-1}, in consecutive stages. In the early stage, a greater G will enhance collisions and coagulation between small particles in water. In the later stage, a lower G will minimize the breakage of the aggregates formed. All of these operational measures are utilized to generate larger flocs that can be readily removed from the water column by the subsequent sedimentation.

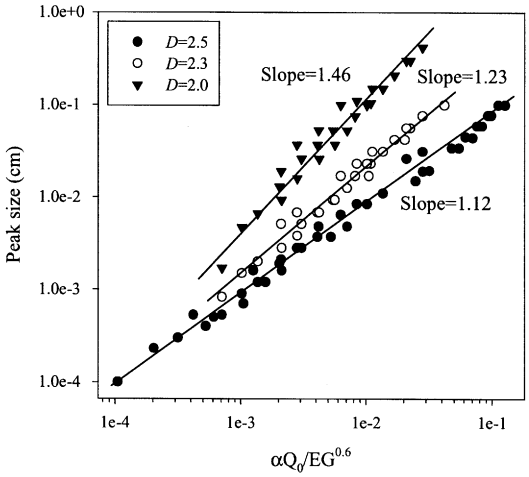

Figure 5. Size of the peak mass concentration in a steady-state size distribution of particles as a function of the group parameter of $\alpha Q_0/EG^{0.6}$ and the fractal dimension.

The group parameter indicates the roles in particle flocculation of the process variables, including the collision efficiency, initial concentration, fluid shear rate, and breakage rate constant.

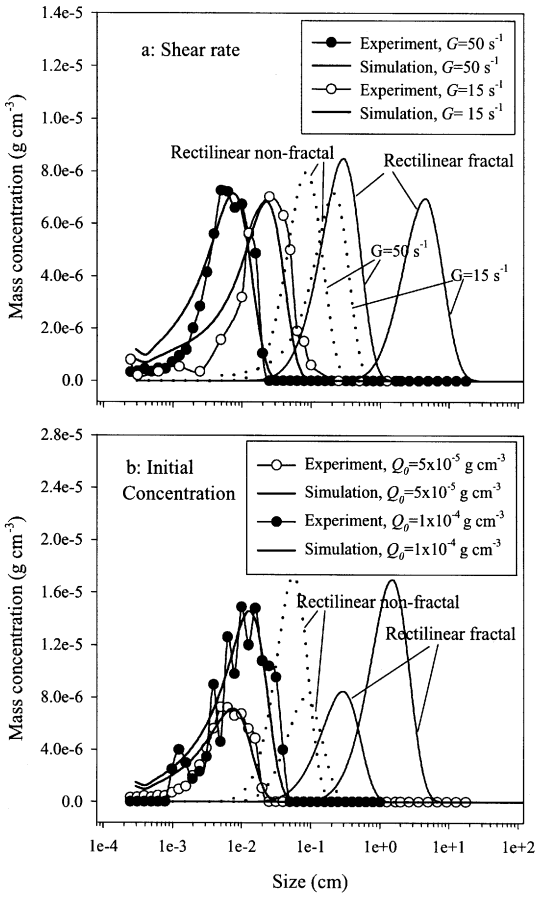

Figure 6. Steady-state particle-size distributions that were observed during the normal flocculation experiments: (a) shear rate changed from $G = 50$ to 15 s^{-1}, $Q_0 = 5 \times 10^{-5}$ g·cm^{-3} and (b) initial concentration changed from $Q_0 = 5 \times 10^{-5}$ to 1×10^{-4} g·cm^{-3}, $G = 50$ s^{-1}, compared to numerical simulations using the curvilinear model with $\alpha = 0.8$ and $D = 2.2$ assumed.

The simulation results from the rectilinear-based models with and without the fractal scaling relationship are also included for additional comparisons.

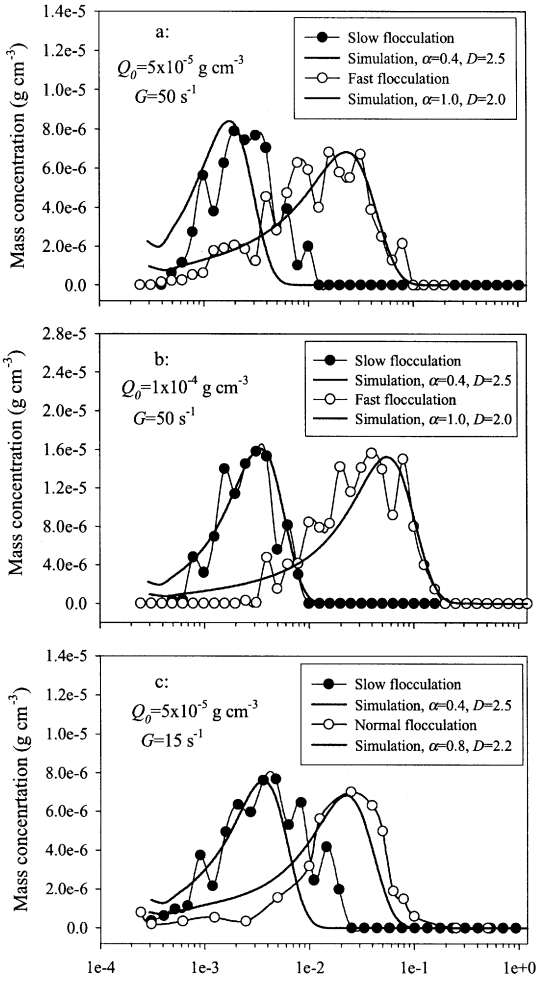

Figure 7. Steady-state particle-size distributions that were observed during the flocculation experiments at $G = 50$ s^{-1} with the initial concentrations of (a) $Q_0 = 5 \times 10^{-5}$ g·cm^{-3}, (b) $Q_0 = 1 \times 10^{-4}$ g·cm^{-3}, and (c) during the experiments with $Q_0 = 5 \times 10^{-5}$ g·cm^{-3} at $G = 15$ s^{-1}, compared to numerical simulations using the curvilinear model.

$\alpha = 0.4$ and $D = 2.5$ assumed for the slow flocculation case, $\alpha = 0.8$ and $D = 2.2$ assumed for the normal flocculation case, and $\alpha = 1.0$ and $D = 2.0$ assumed for the fast flocculation case.

Comparison between the numerical simulation and the experimental study

A series of particle flocculation experiments were carried out to evaluate the predictions of the modeling simulations concerning the effects of various operation variables on the steady-state size distribution. In general, the simulations compared fairly well with the experimental results (Figures 6 and 7). The effects of the shear rate and initial concentration on flocculation were examined for the normal flocculation case with $\alpha = 0.8$ and $D = 2.2$ assumed for the system. When the shear rate decreased from 50 to 15 s^{-1} at an initial concentration of 5.0×10^{-5} g·cm^{-3}, the position of the peak concentration changed from 70 to 300 μm based on the experimental observation, in comparison to the change from 80 to 260 μm based on the numerical simulation. The steady-state size distributions from both the experiment and the simulation were quite close (Figure 6a). As the initial concentration increased from 5.0×10^{-5} g·cm^{-3} to 1.0×10^{-4} g·cm^{-3}, the size of the peak concentration increased from 50 μm to 200 μm during the experiment, while it changed from 70 μm to 160 μm according to the simulation. The peak concentration increased from 7.2×10^{-6} g·cm^{-3} to 1.5×10^{-5} g·cm^{-3} in the experiment, compared to the change from 7.0×10^{-6} g·cm^{-3} to 1.4×10^{-5} g·cm^{-3} in the simulation (Figure 6b). The size of the steady-state peak concentration increased with the initial concentration in a manner that was consistent with those reported by others for activated sludge (Chaignon et al., 2002) and clay particles (Ducoste, 2002). The results of the numerical simulation and the experimental study are in good agreement for the effects of shear rate and

initial concentration on the coagulation–breakage dynamics, which suggests the applicability of the mathematical modeling system that is established in this study. The breakage rate constant of $E = 7.0 \times 10^{-4}$ is also proved to be appropriate for use in modeling the breakage kinetics.

In relation to the experimental results, additional comparisons were made between the simulations based on the present curvilinear-based model and previous rectilinear-based models, including the rectilinear–fractal–breakage model (Serra and Casamitjana, 1998a) and the rectilinear–nonfractal–breakage model (Spicer and Pratsinis, 1996). As indicated earlier, the rectilinear model neglects hydrodynamic interactions and short-range forces between approaching particles. The rectilinear-based kinetic models overpredict particle coagulation rates, resulting in a significant shift of the size distributions to larger particles compared to the experimental observations and the curvilinear-based simulations (Figure 6). In relative terms, the rectilinear–nonfractal–breakage model appeared to describe the flocculation system better than does the rectilinear–fractal–breakage model. The nonfractal assumption ignores the growing pores formed within particle aggregates, giving smaller areas for particle collisions. While the rectilinear assumption overestimates the rates of particle coagulation, the nonfractal assumption underpredicts them. The opposite effects of these two assumptions, however, may offset each other to a certain extent for the prediction of overall coagulation rates. As a result, the flocculation simulation using the rectilinear–nonfractal model could be close to that using the improved curvilinear–fractal approach. It is generally accepted that the curvilinear model is more accurate than the rectilinear model, and that fractal mathematics is better than the Euclidean geometry for the aggregate structure. However, in modeling the flocculation dynamics, both modifications should be applied together. If only fractal scaling is adopted, then the errors in the simulation would be increased rather than reduced when compared with those using the conventional rectilinear and nonfractal model.

Changes in the experimental conditions resulted in different flocculation rates. Based on the experimental measurement at $G = 50\ s^{-1}$, for the slow flocculation case with $\alpha = 0.4$ and $D = 2.5$ assumed, the peak size and concentration were 25 μm and $8.0 \times 10^{-6}\ g \cdot cm^{-3}$ at an initial concentration of $5.0 \times 10^{-5}\ g \cdot cm^{-3}$, while they changed to 30 μm and $1.6 \times 10^{-5}\ g \cdot cm^{-3}$ at a higher concentration of $1.0 \times 10^{-4}\ g \cdot cm^{-3}$. Based on the numerical simulation, the peak size and concentration were 20 μm and $8.3 \times 10^{-6}\ g \cdot cm^{-3}$ for an initial concentration of $5.0 \times 10^{-5}\ g \cdot cm^{-3}$, which changed to 30 μm and $1.6 \times 10^{-5}\ g \cdot cm^{-3}$ for a higher concentration of $1 \times 10^{-4}\ g \cdot cm^{-3}$ (Figure 7). For the slow flocculation case at $G = 50\ s^{-1}$, the simulation and experiment agreed well with each other in terms of the steady-state size distribution. For the fast flocculation case with $\alpha = 1.0$ and $D = 2.0$ assumed, the peak size and concentration were 200 μm and $7.0 \times 10^{-6}\ g \cdot cm^{-3}$ at an initial concentration of $5.0 \times 10^{-5}\ g \cdot cm^{-3}$, while they were 400 μm and $1.6 \times 10^{-5}\ g \cdot cm^{-3}$ at a concentration of $1.0 \times 10^{-4}\ g \cdot cm^{-3}$ during the experiment. In comparison, based on the simulation, the peak size and concentration were 250 μm and $6.8 \times 10^{-6}\ g \cdot cm^{-3}$ for the initial concentration of $5.0 \times 10^{-5}\ g \cdot cm^{-3}$ and 500 μm and $1.4 \times 10^{-5}\ g \cdot cm^{-3}$ for a higher concentration of $1.0 \times 10^{-4}\ g \cdot cm^{-3}$ (Figure 7). An increase in the initial concentration based on either the numerical simulation or the experimental observation generated more large-particle aggregates. For a low shear intensity of $G = 15\ s^{-1}$, the simulation results also agreed reasonably well with the experimental measurements in terms of the steady-state particle-size distribution (Figure 7c).

In natural waters and engineered treatment processes, the characteristic time for the flocculation system to reach the steady state is as important as the final steady-state size distribution. The sooner the flocculation is completed, the more efficient is the unit operation. The characteristic times determined from the simulations of the curvilinear–fractal–breakage model compared well with the experimental observations. For the tests at $G = 50\ s^{-1}$ and initial $Q_0 = 5.0 \times 10^{-5}\ g \cdot cm^{-3}$ (Figure 7a), the fast flocculation reached its steady state after about 1 h and the slow flocculation reached the steady state after 8 h, in comparison to 1.7 and 8.9 h, respectively, predicted by the new curvilinear-based model. Much shorter times were given by the rectilinear-based models, with 0.1 and 0.7 h using the rectilinear–fractal–breakage model and 1.5 and 4.4 h using the rectilinear–nonfractal–breakage model for the respective fast and slow flocculation cases. For the tests with a higher initial $Q_0 = 1.0 \times 10^{-4}\ g \cdot cm^{-3}$ (Figure 7b), the fast and slow flocculation experiments reached the steady state after about 1 h and 7 h, respectively, while the related simulations produced stable size distributions after 1.3 and 6.9 h. Using the rectilinear–fractal–breakage model, the characteristic times were shortened to 0.2 and 0.5 h for the fast and slow flocculation, respectively, while with the rectilinear–nonfractal–breakage model the times were 1.4 and 3.3 h. Similar to the preceding discussion on the position of the steady-state size distribution, the rectilinear model with only the fractal adjustment actually worsens the prediction of the characteristic time when compared with the conventional rectilinear–nonfractal model. For the experiments at $G = 15\ s^{-1}$ (Figure 7c), the characteristic times were around 2 and 13 h for the normal and slow flocculation cases, respectively, which were somewhat shorter than the values of 6.9 and 19.4 h determined from the curvilinear–fractal model.

In general, the best agreement between the simulation and the experiment of the particle-size distribution dynamics was obtained for the slow and normal flocculation cases, followed by the fast flocculation case. The simulation of particle coagulation was based on the assumption that particle attachment only resulted from particle–particle collisions (O'Melia and Tiller, 1993). This, however, may not be true for the fast flocculation process. With the precipitates of overdosed flocculants (30 mg/L) during fast flocculation, other coagulation mechanisms may play a more important role in aggregate formation. A large number of chemical precipitates would enhance coagulation by particle enmeshment or sweep coagulation (Amirtharajah and O'Melia, 1990; American Water Works Association, 1998) rather than by collisions between particles. Large aggregates formed in flocculation systems are found to be highly fractal and porous, which may allow fluid to flow through the aggregate interior (Li and Logan, 1997). The interaggregate flow would increase collision frequencies between the aggregates and suspended small particles, resulting in an overall coagulation rate faster than that predicted by the curvilinear kinetics. In the present study, to reconcile the simulation of particle-size distribution dynamics with the fast flocculation experiment, a collision frequency of $\alpha = 1.0$

had to be employed. Such a high α might not be realistic for an actual particle system, suggesting the possible mechanism of particle collisions brought about by the internal flow through permeable aggregates. This mechanism, however, is not readily available mathematically for inclusion in the coagulation models for process simulations.

Moreover, the highly porous alum precipitates could be weaker than the particle aggregates formed by slow and normal coagulation, and, thus, more vulnerable to breakage (Spicer and Pratsinis, 1996; Serra and Casamitjana, 1998b). A higher breakup rate constant would be better applied to the system of fast flocculation than of normal or slow flocculation. Information on the breakage rate constants for different types of particle aggregates, however, is largely limited. Hence, more experimental studies need to be conducted into the kinetic description of sweep coagulation and the breakage characteristics of flocculate precipitate-based aggregates.

Conclusions

The sectional modeling approach has been advanced to simulate a particle flocculation system that accounts for both the coagulation and breakage processes. The major improvement includes the use of a continuous-size density function instead of a characteristic size for each size section, the applications of a comprehensive curvilinear model developed by Han and Lawler (1992) for the coagulation kinetics, and the fractal scaling relationship for particle aggregates. With the modified modeling methodology, the time evolution in particle-size distribution was well simulated for a pulsed input into a batch flocculator. As indicated by a stationary particle-size distribution with a unique peak mass concentration, the flocculation system could arrive at a dynamic steady state after a period of simulation when coagulation and breakage achieved equilibrium. The simulation results demonstrate that the curvilinear–fractal–breakage approach overcomes the deficiencies of the conventional rectilinear–nonfractal approach. Three distinct breakage distribution functions—binary, ternary, and normal distribution—differ only slightly in the simulation results of the steady-state size distributions. A higher collision efficiency and initial particle concentration and a lower shear rate and breakage rate constant produce a larger population of large-particle aggregates in a flocculation system. A universal parameter for these process variables, $\alpha Q_0/EG^{0.6}$, which regulates the performance of the flocculation process, has been defined. The simulation results indicate that the peak size of the particle-size distribution after flocculation varies with this group parameter to a power of approximately $3/D$. The numerical simulations in terms of the steady-state particle-size distribution and the characteristic time for the system to reach its steady state compared fairly well with the observations of the jar-test flocculation experiments using latex particles. The agreement between the simulation and experimental results suggests that the modeling system can be readily applied in the process simulation of the flocculation units used in water and wastewater treatment.

Acknowledgment

This research was supported by HKU7327/98E from the Research Grants Council of the Hong Kong SAR Government, China.

Notation

A = Hamaker's constant (4.0×10^{-13} g·cm^2·s^{-2})
a, b, c, d = intermediate coefficients used for the calculation of curvilinear reduction factors in Eqs. 16–18
B = sectional coagulation coefficient as defined in Table 1
b = breakage rate constant used in Eq. 6 ($b = 1.6$)
c = constant used in Eq. 4
D = fractal dimension
d_s = solid equivalent diameter of a particle (cm)
E, E' = breakage constants used in Eqs. 6 and 7, respectively
e_{Br}, e_{Sh}, e_{DS} = curvilinear reduction factors related to the rectilinear collision kernels of Brownian motion, fluid shear, and differential sedimentation, respectively
G = shear rate, s^{-1}
g = gravitational constant (981 cm·s^{-2})
H_A, N_g = dimensionless numbers used for the calculation of e_{sh} and e_{DS}, respectively
i, j, k, s = particle-size sections
k = Boltzmann's constant (1.38×10^{-16} g·cm^2·s^{-2}·K^{-1})
l = length of a particle, cm
l_l = length of the larger particle, cm
M = cumulative particle mass distribution, g·cm^{-3}
m, m', m'' = mass of a particle, g
m_f = mean mass of the normal size distribution of fragments
m_{k-1}, m_k = lower and upper bound mass values of section k, g
m_x, m_y = masses of a pair of particles forming a doublet as shown in Table 1
m_z = mass of a broken particle that is larger than the particles in section k, g
$n(m)$ = particle size (mass) density function (#·cm^{-3}·g^{-1})
p_1, p_2, p = intermediate constants related to Eq. 20
Q_k = mass concentration in section k, g·cm^{-3}
Q_0 = initial particle-mass concentration in a flocculation system, g·cm^{-3}
s = breakage rate coefficient
S = sectional breakage coefficient as defined in Table 1
T = absolute temperature, K
t = time, s
U = settling velocity as predicted by Stokes' law, cm·s^{-1}
V = volume of an aggregate, cm^3

Greek letters

α = collision efficiency between colliding particles
β = collision frequency function as predicted by a rectilinear model, cm^3·s^{-1}
$\beta_{Br}, \beta_{Sh}, \beta_{DS}$ = collision frequency functions induced by Brownian motion, fluid shear, and differential sedimentation, respectively, cm^3·s^{-1}
β_{cur} = collision frequency function as predicted by a curvilinear model, cm^3·s^{-1}
γ = fragment-size distribution function
λ = size ratio of two approaching particles ($\lambda \le 1$)
ρ_p, ρ_a, ρ_l = densities of a primary particle, aggregate, and liquid, respectively, g·cm^{-3}
μ = dynamic fluid viscosity of water, g·cm^{-1}·s^{-1}
σ_f = standard deviation of the fragment size distribution

Literature Cited

American Water Works Association, *Water Treatment Plant Design*, 3rd ed., McGraw-Hill, New York, p. 87 (1998).

Adachi, Y., M. Kobayashi, and S. Ooi, "Applicability of Fractals to the Analysis of the Projection of Small Flocs," *J. Colloid Interface Sci.*, **208**, 353 (1998).

Amirtharajah, A., and C. R. O'Melia, "Coagulation Processes: Destabilization, Mixing, and Flocculation," *Water Quality and Treatment*, 4th ed. by American Water Works Association, McGraw-Hill, New York, p. 269 (1990).

Boadway, J. D., "Dynamics of Growth and Breakage of Alum Flocs in Presence of Fluid Shear," *J. Environ. Eng. Div., ASCE*, **104**, 901 (1978).
Chaignon, V., B. S. Lartiges, A. EI Samrani, and C. Mustin, "Evolution of Size Distribution and Transfer of Mineral Particles between Flocs in Activated Sludges: An Insight into Floc Exchange Dynamics," *Water Res.*, **36**, 676 (2002).
Chen, W., R. R. Fisher, and J. C. Berg, "Simulation of Particle Size Distribution in an Aggregation-Breakup Process," *Chem. Eng. Sci.*, **45**, 3003 (1990).
Chung, C. B., S. H. Park, I. S. Han, Y. H. Seo, and B. T. Yang, "Modeling of ABS Latex Coagulation Processes," *AIChE J.*, **44**, 1256 (1998).
Cohen, R. D., "Self-Similar Cluster Size Distribution in Random Coagulation and Breakup," *J. Colloid Interface Sci.*, **149**, 261 (1992).
Coulaloglou, C. A., and L. L. Tavlarides, "Description of Interaction Processes in Agitated Liquid-Liquid Dispersion," *Chem. Eng. Sci.*, **32**, 1289 (1977).
Dasgupta, S., "A Model of Aggregation and Dissociation," *J. Phys. A: Math. Gen.*, **33**, L339 (2000).
Ducoste, J., "A Two-scale PBM for Modeling Turbulent Flocculation in Water Treatment Process," *Chem. Eng. Sci.*, **57**, 2157 (2002).
Fair, G. M., and R. S. Gemmell, "A Mathematical Model of Coagulation," *J. Colloid Interface Sci.*, **19**, 360 (1964).
Flesch, J. C., P. T. Spicer, and S. E. Pratsinis, "Laminar and Turbulent Shear-Induced Flocculation of Fractal Aggregates," *AIChE J.*, **45**, 1114 (1999).
Gardner, K. H., T. L. Theis, and T. C. Young, "Colloid Aggregation: Numerical Solution and Measurements," *Colloids Surf. A: Physiochem. Eng. Aspects*, **141**, 237 (1998).
Gelbard, F., Y. Tambour, and H. H. Seinfeld, "Sectional Representations for Simulating Aerosol Dynamics," *J. Colloid Interface Sci.*, **76**, 541 (1980).
Han, M. Y., and D. F. Lawler, "The (relative) Insignificance of G in Flocculation," *J. AWWA*, **84**, 79 (1992).
Higashitani, K., K. Limura, and H. Sanda, "Simulation of Deformation and Breakup of Large Aggregates in Flows of Viscous Fluids," *Chem. Eng. Sci.*, **56**, 2927 (2001).
Hounslow, M. J., R. L. Ryall, and V. R. Marshall, "A Discretized Population Balance for Nucleation, Growth, and Aggregation," *AIChE J.*, **34**, 1821 (1988).
Jackson, G. A., and S. E. Lochmann, "Modeling Coagulation of Algae in Marine Ecosystems," *Environmental Particles 2*, J. Buffle and H. P. van Leeuwen, eds., Lewis, Boca Raton, FL, p. 387 (1993).
Jackson, G. A., "Using Fractal Scaling and Two-Dimensional Particles Size Spectra to Calculate Coagulation Rates for Heterogeneous Systems," *J. Colloid Interface Sci.*, **202**, 20 (1998).
Johnson, C. P., X. Y. Li, and B. E. Logan, "Settling Velocities of Fractal Aggregates," *Environ. Sci. Technol.*, **30**, 1911 (1996).
Jiang, Q., and B. E. Logan, "Fractal Dimensions of Aggregates Determined from Steady-State Size Distribution," *Environ. Sci. Technol.*, **16**, 303 (1991).
Jiang, Q., and B. E. Logan, "Fractal Dimensions of Aggregates Produced in Laminar and Turbulent Shear Devices," *J. AWWA*, **88**, 100 (1996).
Kostoglou, M., S. Dovas, and A. J. Karabelas, "On the Steady-State Size Distribution of Dispersions in Breakage Processes," *Chem. Eng. Sci.*, **52**, 1285 (1997).
Kusters, K. A., S. E. Pratsinis, S. G. Thoma, and D. M. Smith, "Ultrasonic Fragmentation of Agglomerate Powders," *Chem. Eng. Sci.*, **48**, 4119 (1993).
Lee, D. G., J. S. Bonner, L. S. Garton, A. N. S. Ernest, and R. L. Autenrieth, "Modeling Coagulation Kinetics Incorporating Fractal Theories: A Fractal Rectilinear Approach," *Water Res.*, **34**, 1987 (2000).
Li, D. H., and J. J. Ganczarczyk, "Fractal Geometry of Particle Aggregates Generated in Water and Wastewater Treatment Processes," *Environ. Sci. Technol.*, **23**, 1385 (1989).
Li, X. Y., and B. E. Logan, "Size Distribution and Fractal Properties of Particles During a Simulated Photoplankton Bloom in a Mesocosm," *Deep-Sea Res. II*, **42**, 125 (1995).
Li, X. Y., and B. E. Logan, "Collision Frequencies Between Fractal Aggregates and Small Particles in Turbulently Sheared Fluid," *Environ. Sci. Technol.*, **31**, 1237 (1997).
Li, X. Y., and Y. Yuan, "Collision Frequencies of Microbial Aggregates with Small Particles by Differential Sedimentation," *Environ. Sci. Technol.*, **36**, 387 (2002).
Li, X. Y., and J. J. Zhang, "Numerical Simulation and Experimental Verification of Particle Coagulation Dynamics for a Pulsed Input," *J. Colloid Interface Sci.*, **262**, 149 (2003).
Lu, C. F., and L. A. Spielman, "Kinetics of Floc Breakage and Aggregation in Agitated Fluid Suspensions," *J. Colloid Interface Sci.*, **103**, 95 (1985).
Meakin, P., "Fractal Aggregates," *Adv. Colloid Interface Sci.*, **28**, 249 (1988).
Oles, V., "Shear-Induced Aggregation and Breakage of Polystyrene Latex Particles," *J. Colloid Interface Sci.*, **154**, 351 (1992).
O'Melia, C. R., and C. L. Tiller, "Physicochemical Aggregation and Deposition in Aquatic Environments," *Environmental Particles 2*, J. Buffle and H. P. van Leeuwen, eds., Lewis, Boca Raton, FL, p. 252 (1993).
Packham, R. F., "Some Studies of the Coagulation of Dispersed Clays with Hydrolyzing Salts," *J. Colloid Interface Sci.*, **20**, 81 (1965).
Pandya, J. D., and L. A. Spielman, "Floc Breakage in Agitated Suspensions: Theory and Data Processing Strategy," *J. Colloid Interface Sci.*, **90**, 517 (1982).
Park, S. H., and K. W. Lee, "Asymptotic Particle Size Distributions Attained During Coagulation Processes," *J. Colloid Interface Sci.*, **233**, 117 (2001).
Patil, D. P., J. R. G. Andrews, and P. H. T. Uhlherr, "A Lumped Discrete Population Balance Model for Shear Flocculation-Model Development," *Int. J. Miner. Process*, **50**, 289 (1997).
Peng, S. J., and R. A. Williams, "Direct Measurement of Floc Breakage in Flowing Suspensions," *J. Colloid Interface Sci.*, **166**, 321 (1994).
Potanin, A. A., "On the Mechanism of Aggregation in the Shear Flow of Suspension," *J. Colloid Interface Sci.*, **145**, 140 (1991).
Seinfeld, J. H., *Atmospheric Chemistry and Physics of Air Pollution*, Wiley, New York, p. 275 (1986).
Serra, T., and X. Casamitjana, "Modelling the Aggregation and Breakup of Fractal Aggregates in a Shear Flow," *Appl. Sci. Res.*, **59**, 255 (1998a).
Serra, T., and X. Casamitjana, "Effect of the Shear and Volume Fraction on the Aggregation and Breakup of Particles," *AIChE J.*, **44**, 1724 (1998b).
Spicer, P. T., and S. E. Pratsinis, "Coagulation and Fragmentation: Universal Steady-State Particle Size Distribution," *AIChE J.*, **42**, 1612 (1996).
Spicer, P. T., S. E. Pratsinis, J. Raper, R. Amal, G. Bushell, and G. Meesters, "Effect of Shear Schedule on Particle Size, Density, and Structure in Stirred Tank," *Powder Technol.*, **97**, 26 (1998).
Tambo, N., and H. Hozumi, "Physical Characteristics of Flocs: II. Strength of Flocs," *Water Res.*, **13**, 421 (1979).
Thomas, D. N., S. J. Judd, and N. Fawcett, "Flocculation Modeling: A Review," *Water Res.*, **33**, 1579 (1999).
Veerapaneni, S., and M. R. Wiesner, "Hydrodynamics of Fractal Aggregates with Radically Varying Permeability," *J. Colloid Interface Sci.*, **177**, 45 (1996).
Vigil, R. D., and R. M. Ziff, "On the Stability of Coagulation-Fragmentation Population Balances," *J. Colloid Interface Sci.*, **133**, 257 (1989).
Yeung, A. K. C., and R. Pelton, "Micromechanics: A New Approach to Studying the Strength and Break-Up of Flocs," *J. Colloid Interface Sci.*, **184**, 579 (1996).

Manuscript received Apr. 5, 2002, and revision received Jan. 16, 2003.